The stability of a sheared density interface

G. A. Lawrence
Department of Civil Engineering, University of British Columbia, Vancouver, British Columbia V6T 1W5, Canada

F. K. Browand and L. G. Redekopp
Department of Aerospace Engineering, University of Southern California, Los Angeles, California 90089

(Received 9 January 1990; accepted 20 June 1991)

This study investigates the stability of stratified shear flows when the density interface is much thinner than, and displaced with respect to, the velocity interface. Theoretical results obtained from the Taylor–Goldstein equation are compared with experiments performed in mixing layer channels. In these experiments a row of spanwise vortex tubes forms at the level of maximum velocity gradient which, because of the profile asymmetry, is displaced from the mean interface level. As the bulk Richardson number is lowered from a high positive value the effects of these vortex tubes become more pronounced. Initially the interface cusps under their influence, then thin wisps of fluid are drawn from the cusps into asymmetric Kelvin–Helmholtz billows. At lower Richardson numbers increasingly more fluid is drawn into these billows. The inherent asymmetry of flows generated in mixing layer channels is shown to preclude an effective study of the Holmboe instability. Statically unstable flows (negative Richardson numbers) are subject to the Rayleigh–Taylor instability. However, if the absolute value of the Richardson number is sufficiently small the Kelvin–Helmholtz instability dominates initially.

I. INTRODUCTION

Active study of the stability of a sheared density interface dates back to the work of Taylor[1] and Goldstein.[2] An understanding of this problem is sought after in many branches of science and engineering, since it is fundamental to the generation of turbulence and mixing in stratified flows. Following Taylor[1] and Goldstein[2] we study this problem using piecewise linear approximations to the velocity and density profiles. Mindful of Maslowe's[3] caution that major conclusions should not be made solely on the basis of a study of discontinuous flows, we complement our theoretical investigations with laboratory experiments. Besides providing insight into the mechanisms of instability our results should provide direction for future theoretical, numerical, and laboratory investigations.

The case of an unbounded layer with velocity and density profiles of the form shown in Fig. 1 is analyzed. Two layers of different velocities and densities are separated by interfaces of thickness h and η, respectively. The inflection points of each profile may be displaced a distance d from each other. In many experimental studies of stably stratified shear flows (e.g., Thorpe,[4,5] Scotti and Corcos,[6] and Delisi and Corcos [7]) $\eta \approx h$ and $d \approx 0$. In this case, if the Richardson number is sufficiently low, the primary instability is not significantly different from the Kelvin–Helmholtz instability in unstratified flow, except that the growth of the shear layer is limited by the stabilizing effect of buoyancy. The appearance of smaller scale three-dimensional structures, and the subsequent generation of turbulence and mixing are still being actively studied; see Thorpe[8] and Bayly *et al.*[9]

It may be relevant for some geophysical flows to consider the case where $h \gg \eta$. A stably stratified flow with $h \gg \eta$ and $d = 0$, was studied theoretically by Holmboe[10] who predicted a second mode of instability; we shall call this the Holmboe instability. The Holmboe instability consists of two trains of interfacial waves of equal strength that travel at the same speed, but in opposite directions with respect to the mean flow. This problem has further been studied numerically by Hazel,[11] Smyth *et al.*,[12] and Smyth and Peltier.[13,14] For reasons that will be investigated in the present paper, there have been few experimental realizations of the Holmboe instability. The best visualization is perhaps that of Koop[15] (Fig. 27), reproduced in part in Tritton and Davies[16] (Fig. 8.8).

The present study deals with the more general case where the interface displacement d does not necessarily vanish, and where the flow may be statically unstable. Some experiments for the statically stable case have been performed by Koop and Browand.[17] This work is extended in the present paper by modifying the original facility used by Koop and Browand to enable a more careful study of the initial development of the flow. The instability of the statically unstable case in the absence of shear is known as the

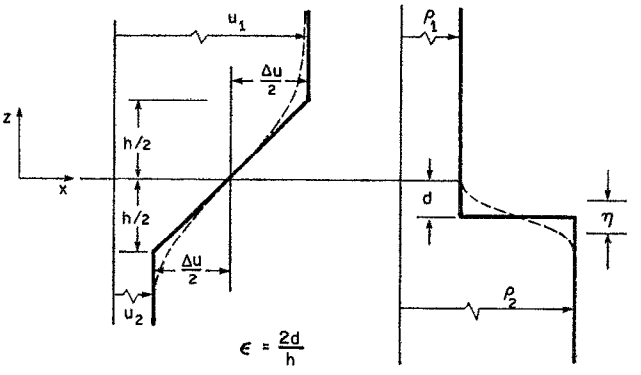

FIG. 1. Definition diagram for the piecewise linear approximations of the velocity and density profiles.

 0899-8213/91/102360-11$02.00

Rayleigh–Taylor instability, and has been studied extensively. For an overview see Sharp.[18] The present study includes an investigation of the sheared Rayleigh–Taylor instability.

II. THEORETICAL DEVELOPMENT

The stability of an inviscid, stratified shear flow depends upon the vertical variation of density $\rho(z)$ and of the mean horizontal velocity $U(z)$. The behavior of a small two-dimensional, monochromatic disturbance of wave number k and wave speed c, is governed by the Taylor–Goldstein equation (named after Taylor[1] and Goldstein[2]):

$$w'' + \{[N^2/(U-c)^2] - [U''/(U-c)] - k^2\}w = 0, \tag{1}$$

where the primes indicate differentiation with respect to z, w is the complex amplitude of the vertical velocity, and the buoyancy frequency $N = \sqrt{(g/\rho)(-d\rho/dz)}$. The variation of density is ignored except in the buoyancy term (the Boussinesq approximation). If there is no mean horizontal velocity then (1) reduces to the Rayleigh–Taylor equation:

$$w'' + [(N^2/c^2) - k^2]w = 0, \tag{2}$$

first studied by Rayleigh[19] [see also Drazin and Reid[20] (p. 324)].

To simplify the analysis the flow is treated as unbounded, and piecewise linear approximations of the velocity and density profiles are made, as indicated in Fig. 1. An advantage of using piecewise linear profiles is that an eigenvalue equation can be derived analytically from the Taylor–Goldstein equation. The densities and velocities of the upper and lower layers are ρ_1, U_1 and ρ_2, U_2, respectively. The velocity difference, $\Delta U = |U_2 - U_1|$, and the density difference, $\Delta\rho = \rho_2 - \rho_1$. The vorticity thickness $h = \Delta U/(dU/dz)_{\max}$ is taken to represent the thickness of the velocity interface. To model flows with $\eta \ll h$, the density is assumed to vary discontinuously at $z = -d$. Using the techniques outlined in Drazin and Reid[20] (Sec. 23) we obtain the following eigenvalue equation:

$$c^4 + a_1 c^3 + a_2 c^2 + a_3 c + a_4 = 0, \tag{3}$$

where

$$a_1 = 2\epsilon,$$

$$a_2 = \beta_+\beta_- - n^2 + \epsilon^2,$$

$$a_3 = 2\epsilon[\beta_+\beta_- - n^2 e^{-\alpha}\sinh(\epsilon\alpha)/\epsilon\alpha],$$

$$a_4 = n^2\{\beta_-^2 + [2(1-\alpha)/\alpha^2]e^{-\alpha}[1-\cosh(\epsilon\alpha)]\} + \epsilon^2\beta_+\beta_-,$$

$$n^2 = 2J/\alpha,$$

and

$$\beta_\pm = [e^{-\alpha} \pm (1-\alpha)]/\alpha.$$

All the variables in the above equation are dimensionless: the complex wave speed $c = (c^* - \bar{U})/\Delta U$, where the the dimensional complex wave speed is $c^* = c_r^* + ic_i^*$, and the mean velocity is $\bar{U} = (U_1 + U_2)/2$; the instability wave number $\alpha = kh$, where $k = 2\pi/\lambda$, and λ is the wavelength; the Richardson number is $J = g'h/\Delta U^2$ (where the modified gravitational acceleration is $g' = g\Delta\rho/\rho_2$); and the profile asymmetry is $\epsilon = 2d/h$.

Equation (3) applies to homogeneous ($J = 0$) and stratified ($J \neq 0$) shear flows, and can be used to investigate the differences between symmetric ($\epsilon = 0$) and asymmetric ($\epsilon \neq 0$) instabilities. Although the main emphasis in the present paper is on asymmetric instabilities in stratified shear flows, we first discuss instabilities in homogeneous flows, and symmetric instabilities in stratified flows. We do this to provide a comparison between the different cases, and to provide some preliminary verification of the validity of (3).

A. Homogeneous flows ($J=0$)

Setting $J = 0$ and $\epsilon = 0$ in (3) gives $c^4 + \beta_+\beta_- c^2 = 0$, so instability occurs if $c^2 = -\beta_+\beta_- = [(1-\alpha)^2 - e^{-2\alpha}]/\alpha^2 < 0$, which, except for a slight change in notation, is the result for a homogeneous shear layer derived by Rayleigh,[21] see also Drazin and Reid[20] (p. 146). In this case small disturbances grow into Kelvin–Helmholtz billows. Setting $J = 0$ and allowing ϵ to vary in the eigenvalue equation (3) yields the additional terms $2\epsilon c^3$, $\epsilon^2 c^2$, $2\epsilon\beta_+\beta_- c$, and $\epsilon^2\beta_+\beta_-$, but if $c^2 = -\beta_+\beta_-$ these terms sum to zero. So if $J = 0$ the result for the homogeneous shear layer holds no matter what value is assumed for ϵ. This is to be expected since the parameter ϵ has no meaning in a homogeneous shear layer.

B. Stratified flows ($J \neq 0$)

1. Symmetric instabilities ($\epsilon = 0$)

When $\epsilon = 0$, Eq. (3) becomes

$$c^4 + a_2 c^2 + a_4 = 0, \tag{4}$$

with $a_2 = \beta_+\beta_- - n^2$ and $a_4 = n^2\beta_-^2$. This is equivalent to the equation derived by Holmboe[10] (Eq. 7.6), and will be called Holmboe's equation. The solutions fall into one of four classes depending on the values of the discriminant $D = a_2^2 - 4a_4$, the Richardson number J, and the coefficient a_2. These classes of solutions correspond to either stable flow or different modes of instability. They will be discussed in turn.

(a) Stable flow. If $D > 0$, $J > 0$, and $a_2 < 0$, then Holmboe's equation has four real solutions and the flow is stable to small perturbations. Figure 2(a) shows the two regions of the J-α plane where these three conditions are satisfied.

(b) Mode I instability. If $D > 0$, $J > 0$, and $a_2 > 0$, then Holmboe's equation has two pairs of purely imaginary roots. There is only one small region, just above the wave-number axis, where this nondispersive instability occurs. The maximum Richardson number is 0.07, and the maximum wave number is 1.28. Only the largest of the imaginary solutions is used to plot the contours of growth rate (αc_i) in Fig. 2(a), since it is this disturbance that will dominate. Although it can be argued that this mode should perhaps be called the Rayleigh mode it is invariably called the Kelvin–Helmholtz mode.

(c) Mode II instability. If $D < 0$ we have the dispersive mode referred to earlier as the Holmboe mode. In this case the solutions to Holmboe's equation are two pairs of complex conjugate roots of the form $c = \pm c_r \pm c_i$. Thus we

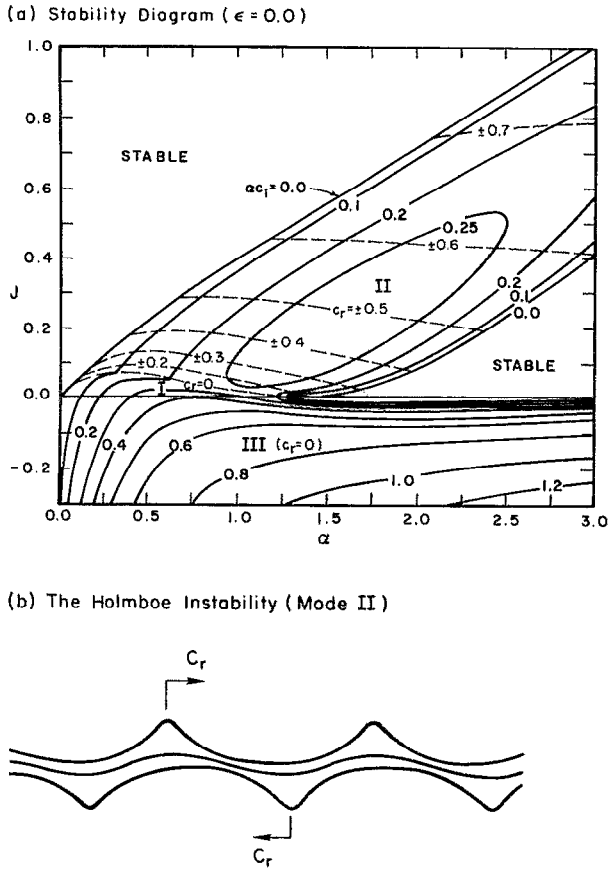

FIG. 2. (a) Stability diagram for symmetric flow ($\epsilon = 0.0$). (——) Contours of constant amplification rate αc_i; (– – –) Contours of constant phase speed c_r. The $c_r = 0$ curve separates the dispersive Holmboe instability (II) from the nondispersive Kelvin–Helmholtz instability (I). Statically unstable flows (III) are subject to both the Kelvin–Helmholtz and Rayleigh–Taylor instabilities. (b) Schematic of the Holmboe instability based on the numerical simulations of Smyth *et al.*[12] The densities of the top, middle, and bottom contours are $\rho_1 + 0.05\Delta\rho$, $(\rho_1 + \rho_2)/2$, and $\rho_2 - 0.05\Delta\rho$, respectively.

have two disturbances, growing at the same rate: a "positive" instability traveling to the right with respect to the mean flow, and a "negative" instability moving to the left at the same relative speed, see Fig. 2(b). The experiments of Browand and Winant[22] and Koop[15] show that, providing the wave amplitude is large enough, fluid is shed from the wave crests in much the same way as the breaking of deep-water surface waves.

Curves of constant amplification rate for the Holmboe mode form closed loops in the upper half-plane, with a maximum amplification rate $\alpha c_i = 0.285$, at $J = 0.195$ and $\alpha = 1.59$. Browand and Wang[23] hypothesized that an increase in growth rate with increasing Richardson number could mean that three-dimensional disturbances, traveling at angles to the stream direction, may be more unstable than two-dimensional disturbances for certain ranges of J and α. Smyth and Peltier[14] have shown that in fact three-dimensional instabilities are the most unstable over an intermediate range of Richardson numbers when the Reynold's number is low. This result does not contradict Squire's[24] theorem that the fastest growing unstable mode of a viscous parallel shear flow is two dimensional, since Squire did not consider stratified flows. This is a possible explanation of the strong three-dimensionality observed in the laboratory by Thorpe[8] and Maxworthy and Browand[25] (Fig. 11).

(d) Mode III instability. For statically unstable flows ($J < 0$) Holmboe's equation has a pair of real and a pair of purely imaginary roots at all wave numbers. The possibility that the resulting nondispersive instability may have characteristics of both the Kelvin–Helmholtz and the Rayleigh–Taylor instability is investigated experimentally in Sec. III.

2. Asymmetric instabilities ($\epsilon \neq 0$)

Although the study of symmetric instabilities is far from complete, it is certainly far more advanced than the study of asymmetric instabilities, which do not appear to have been investigated in any depth prior to the present study. The stability diagrams obtained from (3) for $\epsilon = 0.25, 0.5, 0.75$, and 1.0 are plotted in Fig. 3. For $0 < \epsilon < 1$ the zone of instability for $J > 0$ bifurcates into two limbs that extend to infinity. For the configuration depicted in Fig. 1 the limb closer to the Richardson number axis represents positive instabilities ($c_r^+ > 0$) that protrude into the upper layer; whereas, the limb closer to the wave-number axis represents negative instabilities. Negative instabilities protrude into the lower layer, and their phase speed $c_r^- < -\epsilon$. For homogeneous flows ($J = 0$) we have already shown that the parameter ϵ has no real meaning and $c_r = 0$ as we would expect. To accommodate other flow configurations than that depicted in Fig. 1, we call the layer with the greater velocity shear the "dominant" layer. So for the flow depicted in Fig. 1 the upper layer is the dominant layer.

For statically unstable flows ($J < 0$) only one unstable wave is predicted. Its phase speed is less than that of the positive instability and greater than that of the negative instability, i.e., $-\epsilon < c_r < 0$. This instability has more in common with the positive instability than the negative instability since it moves with the dominant layer like the positive instability, and its growth rate contours are continuous with those of the positive instability.

The solutions to the eigenvalue equation can be written as $c = c_r^+ \pm c_i^+, c_r^- \pm c_i^-$. A general property of equations of the form of (3) is that the sum of their solutions should equal $-a_1$ which, for our case, gives $c_r^+ + c_r^- = -\epsilon$. Therefore, in the region where both instabilities occur, only one contour is needed to represent the phase speeds of both the positive and the negative instabilities, see Fig. 3.

For a given positive value of the Richardson number J the growth rates of both the positive and negative instabilities vary with wave number; however, for $\epsilon > 0$, the positive instability always has the higher maximum growth rate. This means that unless the flow is forced at a particular frequency to favor the growth of the negative instability, the positive instability will dominate. This result provides an explanation for the often observed "one-sidedness" of stratified shear flows referred to in Maxworthy and Browand.[25] In symmetric flows ($\epsilon = 0$) the two instabilities are of equal strength (Fig. 2) yielding Holmboe's instability. As ϵ increases the relative strength of the negative instability de-

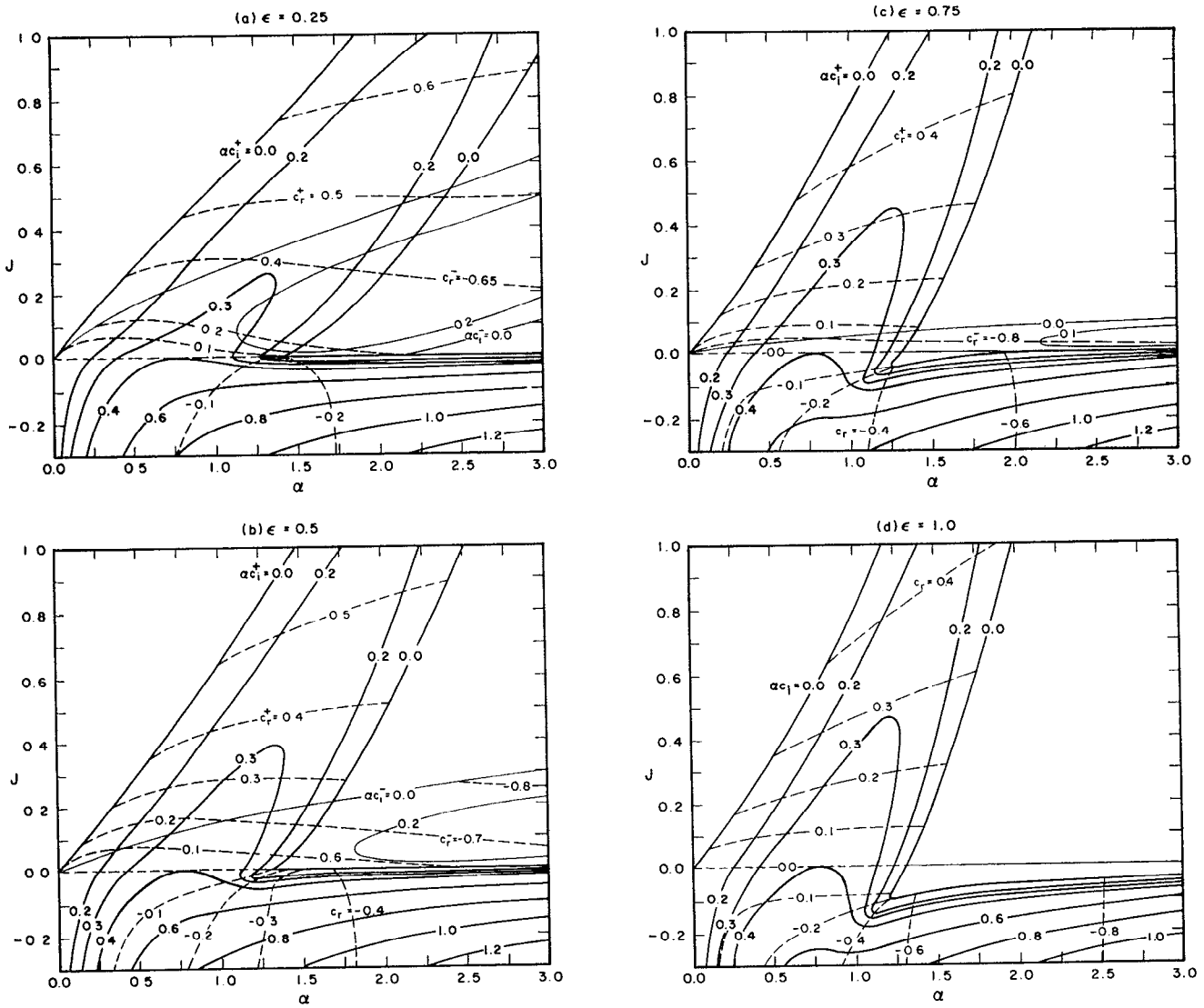

FIG. 3. Stability diagrams for asymmetric flows: (a) $\epsilon = 0.25$; (b) $\epsilon = 0.5$; (c) $\epsilon = 0.75$; (d) $\epsilon = 1.0$. (——) Contours of constant amplification rate αc_i for the positive instability; (——) contours of constant amplification rate αc_i for the negative instability; (– – –) contours of constant phase speed c_r. When both positive and negative instabilities occur at the same time the two phase speeds satisfy $c_r^+ + c_r^- = -\epsilon$.

creases gradually until at $\epsilon = 1$ it disappears completely [Fig. 3(d)].

For high values of ϵ, stability at high wave numbers is predicted for a range of negative Richardson numbers, see Figs. 3(c) and 3(d). Although this somewhat counterintuitive result may be a manifestation of the piecewise linear approximations, it may be that the potential energy that would be gained by a fluid parcel in crossing density surfaces is not sufficient to overcome the kinetic energy lost (see Abarbanel *et al.*[26]). It should also be stressed that even though stability is predicted at high wave numbers, a high degree of instability is predicted at low wave numbers. Aside from this feature the lower half-plane of the stability diagrams does not change dramatically with ϵ.

III. EXPERIMENTS

In this section the results of two sets of experiments investigating different aspects of the stability of a sheared density interface are discussed. One set of experiments was performed in the facility used by Koop and Browand[17] with a 10×10 cm test section. The other set was performed in a modified version of the same facility with a 25×9 cm test section (see Fig. 4). The wider test section was introduced to reduce the relative extent of the region in which the side walls disrupt the two-dimensionality of the flow (see Lasheras and Maxworthy[27]).

An important experimental consideration is the positioning of fine mesh screens at, or near, the trailing edge of the splitter plate. Koop[15] has shown that the initial vorticity thickness h_0, and, therefore, the initial wavelength of the instability, can be varied by repositioning these screens, since they partially remove the boundary layers generated by the splitter plate. Results from two facilities are used in this study because of the difficulty of repositioning the screens once an experimental facility has been built.

The aim of the experiments performed in the modified

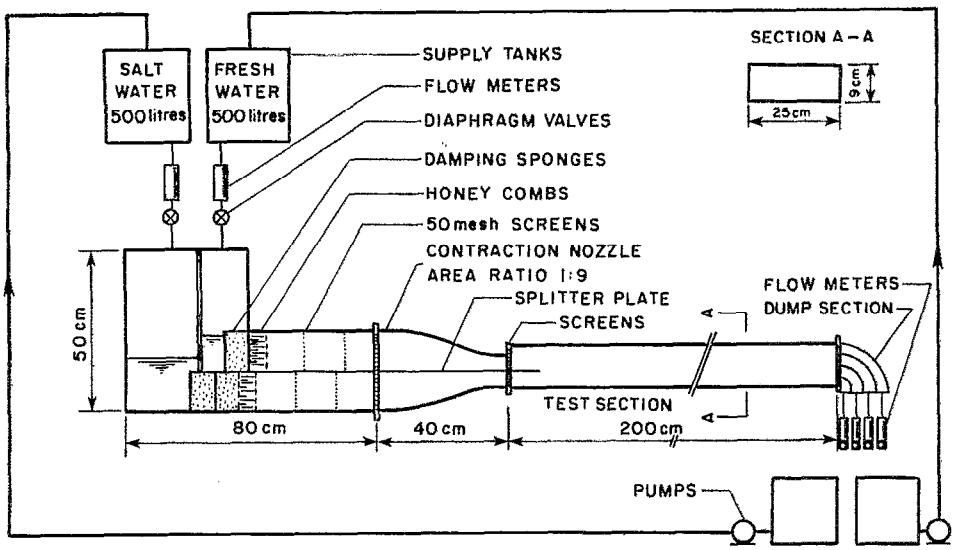

FIG. 4. Experimental apparatus. The original facility built by Koop and Browand[17] had a 10×10 cm test section; whereas, the modified facility has a 25×9 cm test section.

facility was to examine the initial growth of the mixing layer in detail. To facilitate this, the vorticity thickness was made as large as possible under the constraint that the linear stability theory presented above for an unbounded flow still be appropriate for the initial growth of the shear layer. The results of Hazel[11] show that the flow can be regarded as unbounded if the ratio of the total depth to the initial vorticity thickness is 10 or greater. For the experiments performed in the modified facility the total depth of flow was 8.2 cm (4.1 cm for each layer) and the initial vorticity thickness was approximately 0.6 cm, satisfying the above condition. The resulting instabilities had a wavelength of about one-half the total depth of flow. The relatively limited depth of flow inhibited the pairing of successive billows, further enhancing our ability to study the initial instability in detail.

Experiments were performed in the original facility to examine the evolution of the mixing layer to a much later stage. The ratio of the total depth to the initial vorticity thickness was much greater than in the modified facility and pairing was not suppressed by the limited depth of flow. Both statically stable ($J_0>0$) and statically unstable ($J_0<0$) flows were studied. In the statically stable flows growth of the mixing layer by pairing was suppressed by buoyancy rather than the limited depth of flow. In the statically unstable flows the mixing layer initially grew by pairing, but farther downstream the Rayleigh–Taylor instability dominated.

In both facilities, the growth of the shear layer, and the presence of growing boundary layers on the walls of the channel, result in an increasing Richardson number in the streamwise direction. We shall categorize each experiment by the initial value of the Richardson number, $J_0=g'h_0/\Delta U_0^2$, where the subscript 0 denotes initial conditions. For experiments performed in the original facility the initial vorticity thickness h_0 was measured 1 cm downstream of the splitter plate. For experiments performed in the modified facility h_0 was taken to be five times the calculated momentum thickness of the faster layer at the trailing edge of the splitter plate.

The initial profile asymmetry ϵ_0 was determined to be approximately 0.5 in both facilities. The stability diagram for $\epsilon=0.5$ [Fig. 3(b)] shows that the positive instability has much higher maximum amplification rates than the negative instability at all Richardson numbers. Furthermore, the most amplified negative instability occurs at higher wave numbers, and is therefore more highly damped by viscosity, which is ignored in the above analysis. As a consequence we expect "one-sided" flows in which the positive instability dominates. The importance of viscosity is reflected in the value of the shear Reynolds number, $\mathrm{Re}=\Delta U h/\nu$, where ν is the kinematic viscosity of water. A compromise had to be made between obtaining a flow with a high Reynolds number, and a "clean" flow (i.e., one in which the initial flow was as close to two dimensional as possible). This compromise resulted in shear Reynolds numbers between 60 and 300.

A. Results of experiments performed in the modified facility

The flow shown in Fig. 5 is typical of that obtained in the modified facility. In this case $g'=0.13$ cm/sec^2, $h_0=0.6$ cm, $d_0\approx0.3$ cm, $U_1=3.7$ cm/sec, and $U_2=1.7$ cm/sec. These values give $J_0=0.2$, $\epsilon_0\approx0.5$, and $\mathrm{Re}_0=100$. The white lines on the bottom of the flume are 5 cm apart. Flow is from left to right, with a faster upper layer. Fluorescein particles are dissolved in the lower layer to make it visible. Injection of a thin stream of dye about 3 mm above the trailing edge of the splitter plate reveals the presence of concentrated spanwise vorticity in the dominant upper layer (no such concentration of vorticity was found in the lower layer; the flow parameters were in fact selected to avoid significant lower layer vorticity, since we would have then been studying an asymmetric wake rather than a shear layer). These vortex tubes remain above the interface (i.e., $\epsilon>0$) and cause the interface to cusp, but not necessarily billow, into the dominant layer. From Fig. 3(b) we see that the most amplified wave number $\alpha_m=1.1$ for $\epsilon=0.5$ and $J=0.2$, which for a vorticity thickness $h=0.6$ cm gives a predicted

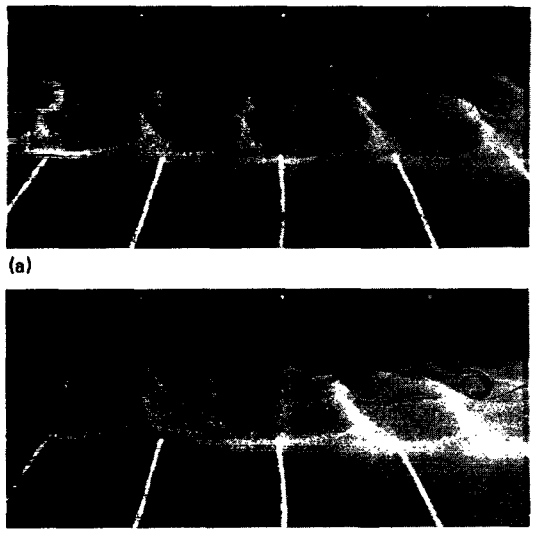

FIG. 5. Photographs taken a few seconds apart of a thin stream of dye injected about 3 mm above the splitter plate showing the presence of spanwise vortex tubes. Note that in (b) two vortices are about to pair. The white lines on the bottom of the flume are 5 cm apart. The distances downstream of the trailing edge of the splitter plate are marked in centimeters. Flow is left to right with a faster upper layer.

wavelength $\lambda = 3.8$ cm. This prediction compares favorably with the observed mean wavelength of 4 cm. Although the two photographs presented in Fig. 5 were taken only a few seconds apart, they are slightly different, since in Fig. 5(b) two vortex tubes are trying to pair.

Side views of five experiments performed to show the effect of varying the Richardson number are given in Fig. 6. The flow conditions are the same as in the experiment depicted in Fig. 5, except that $g' = 0.4$ cm/sec^2, and in each successive experiment the velocity of the upper layer is increased resulting in a decreasing Richardson number. The flow is visualized using laser-induced fluorescence. As the initial Richardson number is decreased the flow becomes more unstable. When $J_0 = 0.3$ [Fig. 6(a)] the interfacial disturbance is approximately sinusoidal and grows very slowly in the downstream direction. At $J_0 = 0.12$ [Fig. 6(b)] the instability is initially sinusoidal, but farther downstream cusps are drawn into the dominant layer under the action of the spanwise vortex tubes. At $J_0 = 0.09$ [Fig. 6(c)] a series of cusps form from which thin billows are drawn. At $J_0 = 0.06$ and 0.05 [Figs. 6(d) and 6(e)] the strength of these asymmetric Kelvin–Helmholtz billows increases drawing more fluid into the dominant layer. Even at these low Richardson numbers the effect of buoyancy is evident in that the amount of fluid drawn into the billows is much less than in the homogeneous case, and some of the billows actually become detached. Smyth[28] and Smyth *et al.*[12] have studied the evolution of sheared two-layer flows numerically, generating flows that closely resemble those shown in Fig. 6.

In general, the first instability forms earlier as the Richardson number is increased; however, there is an inconsistency in that billows appear earlier in the flow with $J_0 = 0.09$ than in the flows with $J_0 = 0.05$ and 0.06. This is probably due to a disturbance to the channel as the photograph of the $J_0 = 0.09$ flow was taken. It is worth noting that farther downstream the lower Richardson number flows are more vigorous.

If we could have reduced the profile asymmetry we might have expected to observe the negative instability increasing in strength until, at $\epsilon = 0$, it became as strong as the positive instability. This may have occurred in the experiments of Browand and Winant[22] and Koop.[15] In these experiments (performed in the original facility) $\epsilon_0 \approx 0.5$, and asymmetric Kelvin–Helmholtz instabilities form. These in-

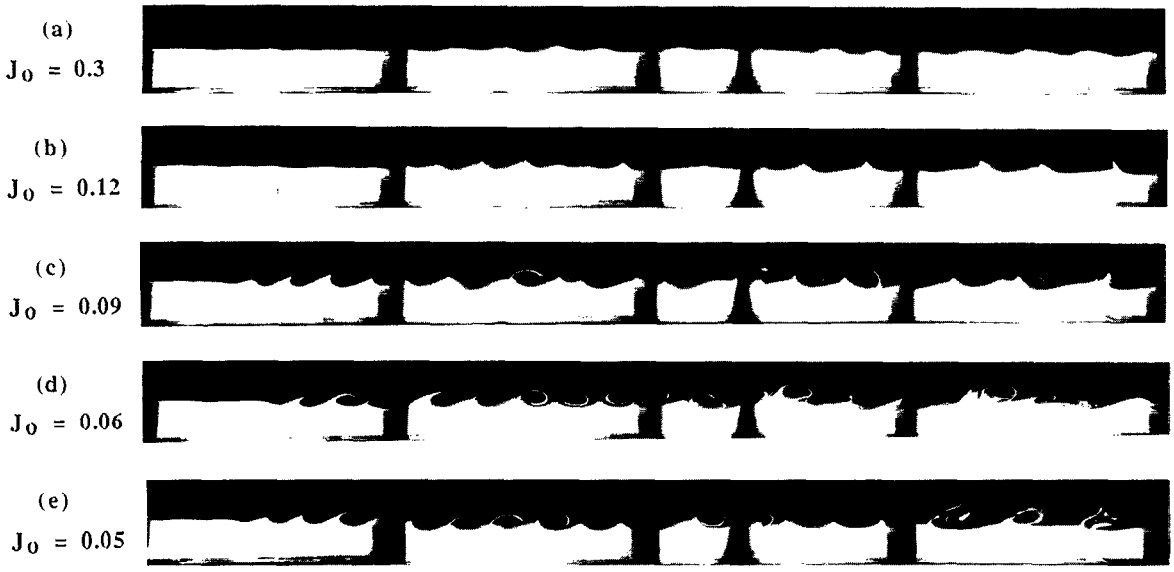

FIG. 6. Side views of experiments performed to investigate the effect of decreasing initial Richardson number J_0. Flow is left to right. The field of view of each photograph is approximately 25 cm. The four photographs for each experiment are not taken simultaneously. The left-hand sides of each of the photographs placed horizontally are at $x = 0$, 20, 40, and 60 cm, respectively.

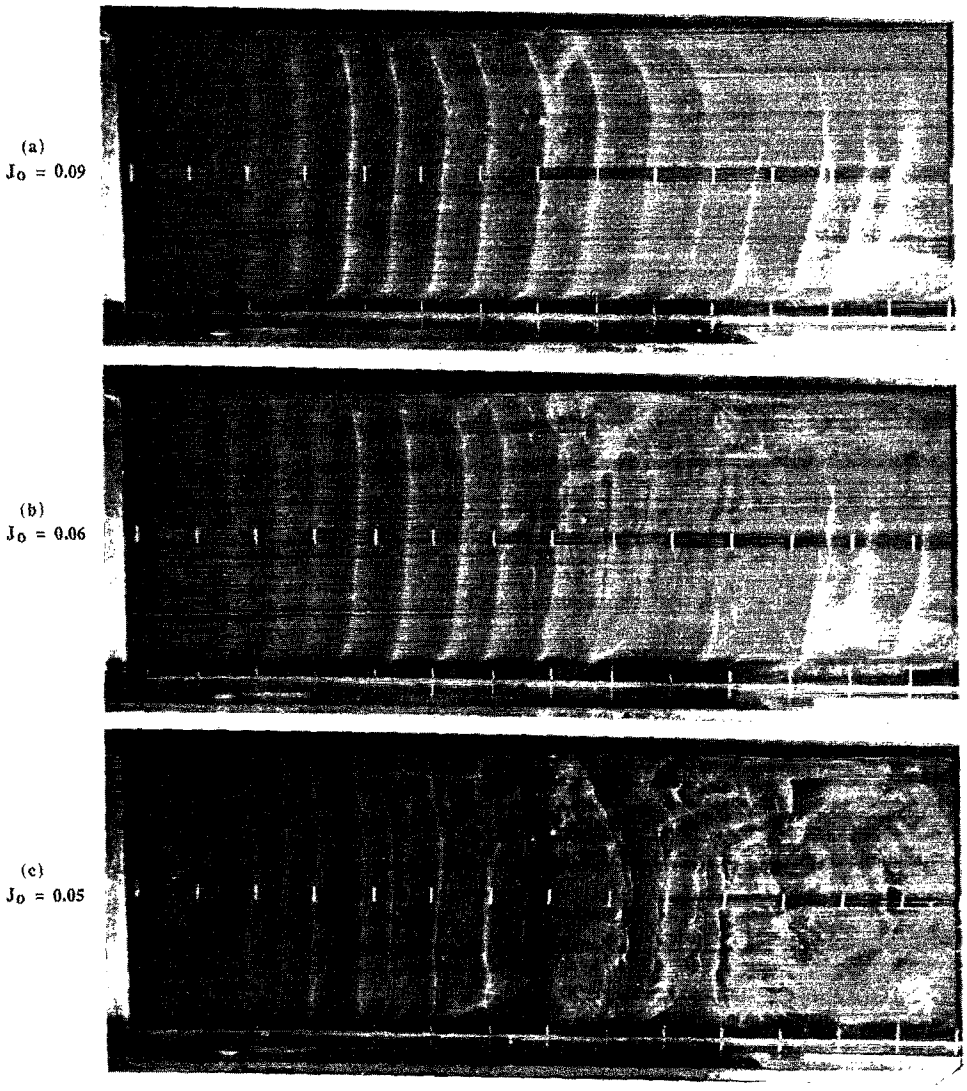

FIG. 7. Plan views of experiments with $J_0 = 0.09$, 0.06, and 0.05, respectively. Flow is left to right. The markings on the bottom of the flume are spaced at 5 cm intervals. The trailing edge of the splitter plate is visible on the left-hand side of each photograph.

stabilities go through a period of growth followed by collapse. In addition, as the flow moves downstream, the value of ϵ drops until, toward the end of the test section, it approaches zero. This variation in profile asymmetry was presumably due to changes in the mean velocity and density profiles as a result of the growth of the mixing layer and the boundary layers on the channel walls. By the time ϵ approaches zero the asymmetric Kelvin–Helmholtz billows have collapsed and the Holmboe instability appears. The conclusion of Browand and Winant[22] that mixed fluid is generated when the positive and negative components of the Holmboe instability pass through each other has yet to be studied in any detail. For a more effective study of the Holmboe instability, experiments need to be devised that do not exhibit the initial profile asymmetry characteristic of mixing layer flows.

In Figs. 6(c)–6(e) it is seen that once billowing has occurred the flow becomes more irregular. This is due to the growth of three-dimensional instabilities that become more apparent when the flow is viewed from above (see Fig. 7). In each experiment the initial instability is almost two dimensional except for the effect of the side walls (see Lasheras and Maxworthy[27]) and of smaller perturbations across the width of the flume. These perturbations may be triggered by the presence of uncontrolled disturbances introduced upstream of the test section. The flow was observed to be very sensitive to the presence of tiny air bubbles trapped behind the screens. Although great care was taken to remove these air bubbles it was not always possible. However, the regular spacing of these perturbations exhibited in Fig. 7 suggests the presence of secondary instabilities. Such instabilities are the subject of considerable recent investigation; see Bayly *et al.*[9] for a review of various proposed mechanisms. Whatever the source of these three-dimensional perturbations, they become more pronounced as billows form. Furthermore, pairing may occur despite the inhibiting effect of the relatively shallow depth of flow. If pairing does occur the vortex tubes are rapidly stretched and convoluted resulting in the flow becoming three dimensional down to the finest scales, as in Fig. 7(c).

The transition from two-dimensional to three-dimensional flow is also revealed in end views of the flow. In Fig. 8 a flow with $J_0 = 0.05$ has been illuminated by a sheet of light extending across the width of the flow. The photographs

FIG. 8. End views of an experiment with $J_0 = 0.05$ illustrating the development of three-dimensional instabilities. (a) $x = 20$ cm, (b) $x = 25$ cm, (c) $x = 35$ cm, and (d) $x = 75$ cm.

have been taken from downstream of the light sheet and slightly above and to the right of the flow. Therefore they are slightly distorted (e.g., the flow appears shallower than it actually is due to refraction). Nevertheless, the important features of the flow are evident. At $x = 20$ cm [Fig. 8(a)] there are slight variations in interface height across the width of the flume with more pronounced effects near the side walls. By $x = 25$ cm [Fig. 8(b)] the transverse perturbations have increased substantially. Once the flow starts to billow at $x = 35$ cm [Fig. 8(c)] a further source of three-dimensionality becomes apparent. The dense fluid in the billow is statically unstable with respect to the fluid below it, and is consequently subject to convective instability. Further downstream the flow becomes highly three dimensional, as shown in Fig. 8(d) taken at $x = 75$ cm.

The validity of the theory presented in Sec. II can be partially tested by comparing the observed wavelength of the instability (before pairing) with that of the most amplified wave given in Fig. 3(b). For the experiments shown in Figs. 7(a), 7(b), and 7(c) (with $\epsilon_0 \approx 0.5$, $J_0 = 0.09$, 0.06, and 0.05, and $h_0 = 0.60$, 0.58, and 0.56 cm, respectively), the predicted wavelengths are 4.1, 4.1, and 4.0 cm, respectively. That these predicted values compare very favorably with the experiments can be seen from Fig. 6 by noting that the markings on the bottom of the flume are 5 cm apart.

B. Results of experiments performed in the original facility

The evolution of the mixing layer was examined in the original facility over a wide range of Richardson numbers ($-0.5 \leqslant J_0 \leqslant 0.2$). Quantitative observations of the mean growth of the mixing region are given in Fig. 9. The horizontal axis is the distance downstream from the splitter plate, normalized by the initial vorticity thickness and the velocity ratio, $R = \Delta U/(U_1 + U_2)$. The inclusion of R is necessary to properly scale experiments having different velocity ratios (see Ho and Huerre[29]). The vertical axis is the thickness of the density distribution, η, normalized by the initial vorticity thickness h_0. The statically stable cases are a replot of data

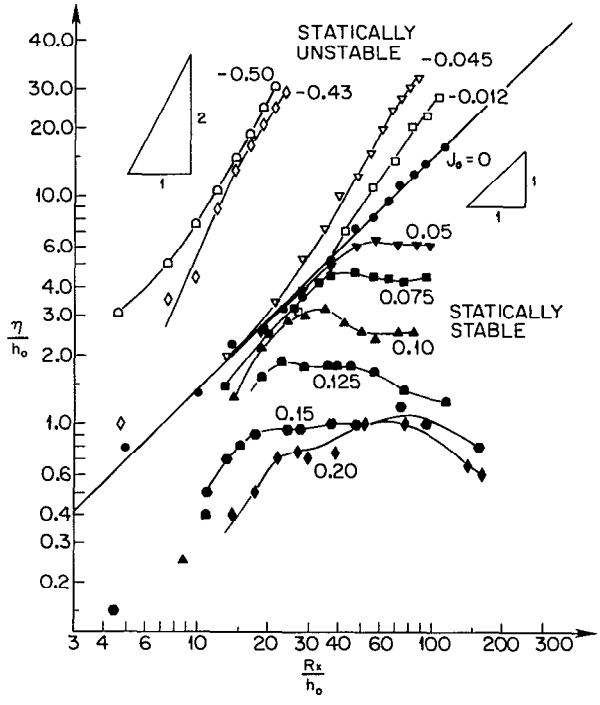

FIG. 9. Measurements of growth rates in both stably and unstably stratified shear layers.

taken from Koop and Browand,[17] and represent observations taken from conductivity probe measurements. The reader is referred to Koop and Browand for further details of these experiments. For the statically unstable cases, the local values of η are approximated as one-half the maximum layer thickness obtained from 16 mm films averaged over several separate runs. The filled circles and the solid line mark the unstratified case, $J = 0$, which effectively separates the results for static stability and instability.

1. Statically stable flows ($J_0 > 0$)

In each of the statically stable experiments all the flow variables were held constant (i.e., $U_1 = 10.95$ cm/sec, $U_2 = 3.2$ cm/sec, $h_0 = 0.38$ cm, $R_0 = 1.1$, and $\mathrm{Re}_0 = 300$), except the initial Richardson number, which was varied between 0.05 and 0.2 by changing the density difference between the two layers. For small positive values of static stability, the layer thickness follows the homogeneous layer growth for some distance, after which there is a rather sharp transition and almost no subsequent growth. The layer thickness may even decrease in the region where the largest scale features are observed to be destroyed by interaction with the buoyancy field. For J_0 values larger than about 0.1, the flow appears to be everywhere dominated by buoyancy and no region of homogeneous growth exists. Note that this result is consistent with the observations made in the modified facility (see Fig. 6).

2. Statically unstable flows ($J_0 < 0$)

For small, statically unstable, density differences, there is an initial region of growth comparable to the unstratified case, as one would expect. In fact, for sufficiently small values of J_0, the sign of J_0 is initially unimportant, and the experimental results display this symmetry. Downstream there is a transition to a more rapid rate of growth. This transition occurs progressively closer to the origin as J_0 takes on larger negative values. For the value $J_0 = -0.43$, the flow has completely departed from the homogeneous behavior, and seems to be growing from the origin approximately as the square of the downstream distance. This result is easily understood. For large statically unstable density differences, the velocity difference, Δu, is dynamically unimportant and η can be expected to become independent of this quantity. The only dependence that will remove Δu is

$$\eta/h_0 = AJ_0(Rx/h_0)^2. \tag{5}$$

By setting $x/\overline{U}$ equal to the elapsed time t, this result can be reduced to its simplest form,

$$\eta = A/4g't^2. \tag{6}$$

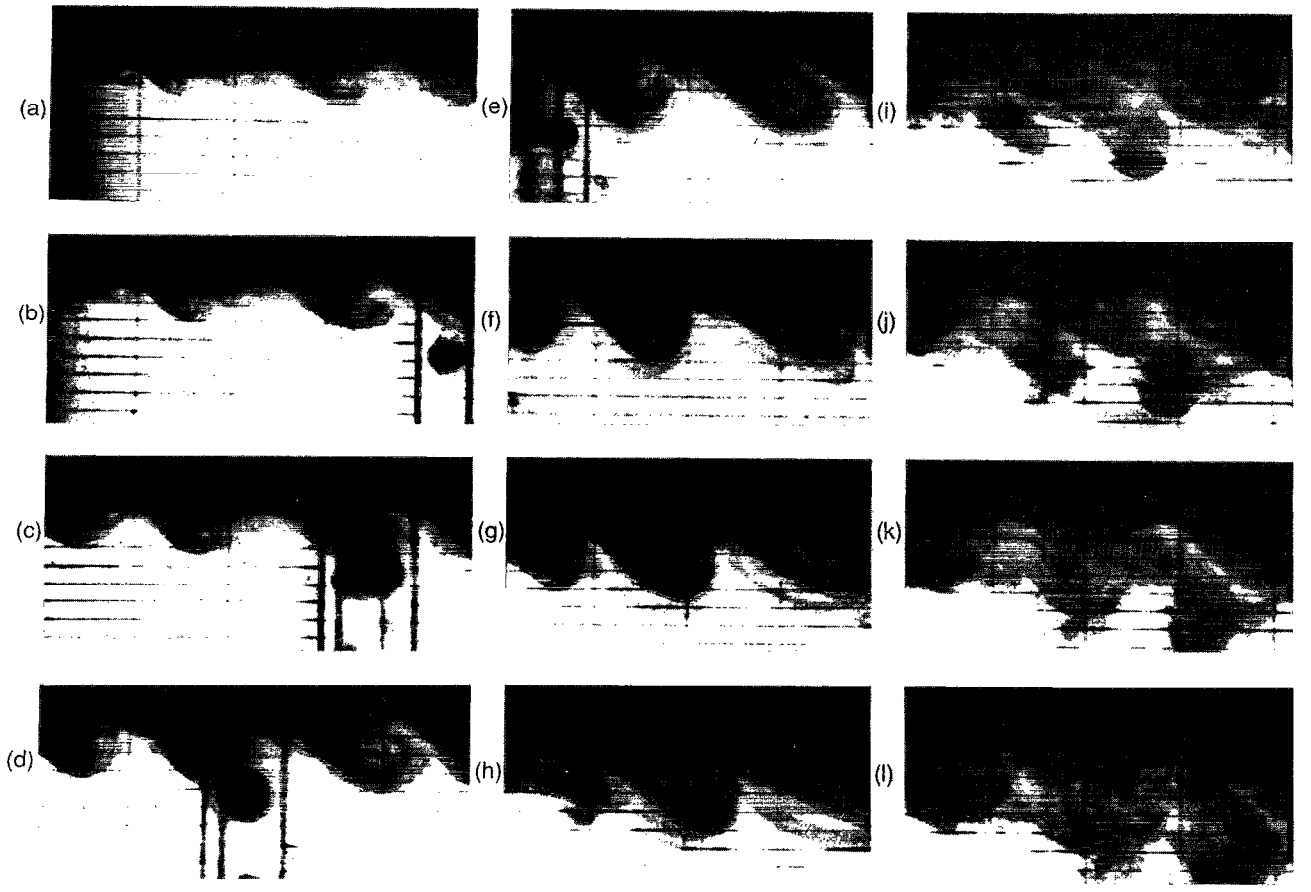

FIG. 10. Development of instability in a flow with $J_0 = -0.03$. The fluid in the upper layer is slightly heavier than that in the lower layer. The camera is moving at approximately the mean velocity, so that the development of individual billows can be observed. The flow is left to right, with the lower layer moving faster. The photographs were taken at intervals of 0.5 sec.

For the experiments with $J_0 = -0.43$ and -0.5, the layer thickness eventually increases simply as a result of a vertical acceleration of the two streams, which is proportional to the reduced gravitational acceleration g'. The constant A is determined to be approximately 0.14, but experiments over a larger range of J_0 would be needed to give more confidence in the numerical value. However, it is very encouraging to note that Read[30] recommends the same value on the basis of experiments on the Rayleigh–Taylor instability performed under very different conditions. Read[30] subjected fluids with ρ_1/ρ_2 from 1.6 to 600 to accelerations of up to $75g$.

The development of instabilities in a flow generated in the original facility with $J_0 = -0.03$ is shown in Fig. 10. The flow is from left to right with the lower layer moving faster. The pictures in Fig. 10 are taken at 0.5 sec intervals from a 16 mm film of the flow. The camera moves with the flow at approximately the mean velocity so that the development of individual billows can be followed. The grid placed on the back of the channel has a horizontal spacing of 2.5 cm and a vertical spacing of 0.5 cm. Near the origin [Figs. 9(a)–9(f)], the flow develops Kelvin–Helmholtz billows as if it were a statically stable shear layer, but eventually buoyancy forces enhance rather than retard the growth. When the scale of the structure is sufficiently large for buoyancy to become important, the upper layer fluid being entrained by the vortices simply continues its downward motion and ultimately becomes a large mushroom-shaped structure [Fig. 9(g)–9(l)]. The spanwise breakdown of the predominantly two-dimensional vortex structure, into what must be a highly three-dimensional mushroomlike Rayleigh–Taylor instability, was not examined.

IV. SUMMARY AND CONCLUSIONS

The stability of stratified shear flows with a density interface much thinner than, and displaced with respect to, the velocity interface has been studied theoretically and experimentally. Solving the Taylor–Goldstein equation for piecewise-linear approximations to the velocity and density profiles yields an eigenvalue equation of the form

$$c^4 + a_1 c^3 + a_2 c^2 + a_3 c + a_4 = 0, \tag{3}$$

where c is the complex wave speed. The coefficients of this equation are functions of the profile asymmetry ϵ, the bulk Richardson number J, and the wave number α. For $J = 0$ Eq. (3) reduces to Rayleigh's equation, and for $\epsilon = 0$ it reduces to Holmboe's equation.

For statically stable flows ($J > 0$) there are two possible unstable waves that travel in opposite directions with respect to the mean flow. The "positive" instability ($c_r^+ > 0$) protrudes into the dominant layer (i.e., the layer with the greater velocity shear). The "negative" instability ($c_r^- < -\epsilon$) protrudes into the other layer. The general solution of (3) requires that $c_r^+ + c_r^- = -\epsilon$. For $\epsilon > 0$ the positive instability always has the greater predicted maximum amplification rate for any given Richardson number. Thus the instability predicted by Holmboe,[10] consisting of positive and negative instabilities of equal strength traveling at the same speed, but in opposite directions with respect to the mean flow, will only occur when $\epsilon = 0$. For statically unstable flows ($J < 0$) linear theory predicts only one unstable wave. Its phase speed is given by $-\epsilon < c_r < 0$. This instability has more in common with the positive instability than the negative instability, since it moves with the dominant layer like the positive instability, and its growth rate contours are continuous with those of the positive instability.

The above results were partially confirmed by experiments performed over a wide range of Richardson numbers in a mixing layer channel where the initial asymmetry $\epsilon_0 \approx 0.5$. In these experiments only the positive instability was observed. At Richardson numbers greater than 0.1 the nonlinear response of the flow to this positive instability was the formation of cusps protruding into the dominant layer. At Richardson numbers less than 0.1 thin wisps of fluid were drawn into the dominant layer by a series of vortex tubes located within the dominant layer and stretching across the flow. The flow begins to resemble Kelvin–Helmholtz billowing in an homogeneous flow, except that the flow is not symmetric about the mean interface level. Only a small volume of fluid is drawn into the dominant layer by these asymmetric Kelvin–Helmholtz billows, and occasionally these billows become detached. Despite the obvious limitations of the theory, e.g., the use of piecewise linear approximations and the assumption of inviscid flow, the predicted wavelengths of the instabilities match the experimental measurements remarkably well.

Holmboe's instability was not observed in any of the experiments, because of the initial profile asymmetry. Experiments need to be devised to avoid this asymmetry before the Holmboe instability can be studied effectively.

For statically unstable flows ($J < 0$) the flow initially behaves like an homogeneous shear layer, but eventually buoyancy forces dominate and the Rayleigh–Taylor instability is observed with growth rates that match those observed in previous experiments on the Rayleigh–Taylor instability.

ACKNOWLEDGMENTS

The authors would like to acknowledge the assistance of Professor Juan Lasheras, Mr. Laurent Guez, Professor Tony Maxworthy, Dr. Geoff Spedding, Mr. Z. Zhu, and Mr. H. Choi for their help at various stages of this study. An earlier version of this paper was presented at the Third Stratified Flows Symposium held on 3–5 February 1987 in Pasadena, California.

Financial support from the U.S. Office of Naval Research's Fluid Mechanics and Oceanography Programs and the Canadian Natural Sciences and Engineering Research Council is gratefully acknowledged.

[1] G. I. Taylor, Proc. R. Soc. London Ser. A **132**, 499 (1931).
[2] S. Goldstein, Proc. R. Soc. London Ser. A **132**, 524 (1931).
[3] S. A. Maslowe, in *Hydrodynamic Instabilities and the Transition to Turbulence*, edited by H. L. Swinney and J. P. Gollub (Springer-Verlag, Berlin, 1985), 2nd ed.
[4] S. A. Thorpe, Boundary Layer Meteorol. **5**, 95 (1973).
[5] S. A. Thorpe, J. Fluid Mech. **61**, 731 (1973).
[6] R. S. Scotti and G. M. Corcos, J. Fluid Mech. **52**, 499 (1972).
[7] D. Delisi and G. M. Corcos, Boundary Layer Meteorol. **5**, 121 (1973).
[8] S. A. Thorpe, J. Geophys. Res. **92**, 5231 (1987).

[9] B. J. Bayly, S. A. Orszag, and T. Herbert, Annu. Rev. Fluid Mech. **20**, 359 (1988).
[10] J. Holmboe, Geofys. Publ. **24**, 67 (1962).
[11] P. Hazel, J. Fluid Mech. **51**, 39 (1972).
[12] W. D. Smyth, G. P. Klaassen, and W. R. Peltier, Geophys. Astrophys. Fluid Dyn. **43**, 181 (1988).
[13] W. D. Smyth and W. R. Peltier, J. Atmos. Sci. **46**, 3698 (1989).
[14] W. D. Smyth and W. R. Peltier, Geophys. Astrophys. Fluid Dyn. **52**, 249 (1990).
[15] C. G. Koop, University of Southern California, Department of Aerospace Engineering Report No. USCAE 134.
[16] D. J. Tritton and P. A. Davies, in Ref. 3.
[17] C. G. Koop and F. K. Browand, J. Fluid Mech. **93**, 135 (1979).
[18] D. H. Sharp, Physica D **12**, 3 (1984).
[19] Lord Rayleigh, Proc. London Math. Soc. **14**, 170 (1883).
[20] P. G. Drazin and W. H. Reid, *Hydrodynamic Stability* (Cambridge U.P., Cambridge, 1981).
[21] Lord Rayleigh, *The Theory of Sound* (Macmillan, London, 1896), 2nd ed. Vol. 2, p. 393.
[22] F. K. Browand and C. D. Winant, Boundary Layer Meteorol. **5**, 67 (1973).
[23] F. K. Browand and Y. H. Wang, *International Symposium on Stratified Flows*, Novosibirsk, 1972 (ASCE, New York, 1972).
[24] H. B. Squire, Proc. R. Soc. London Ser. A **142**, 621 (1933).
[25] T. Maxworthy and F. K. Browand, Annu. Rev. Fluid Mech. **7**, 273 (1975).
[26] H. D. I. Abarbanel, D. D. Holm, J. E. Marsden, and T. Ratiu, Phys. Rev. Lett. **52**, 2352 (1984).
[27] J. C. Lasheras and T. Maxworthy, *Turbulent Shear Flows 5*, edited by F. Durst (Springer-Verlag, Berlin, 1987), p. 124.
[28] W. D. Smyth, M.Sc. thesis, Department of Physics, University of Toronto, 1987.
[29] C.-M. Ho and P. Huerre, Annu. Rev. Fluid Mech. **16**, 365 (1984).
[30] K. I. Read, Physica D **12**, 45 (1984).